Computers and Mathematics with Applications 58 (2009) 975–986

Contents lists available at ScienceDirect

Computers and Mathematics with Applications

journal homepage: www.elsevier.com/locate/camwa

A lattice Boltzmann framework to simulate boiling water reactor core hydrodynamics

Prashant K. Jain [a,*], Adrian Tentner [b], Rizwan-uddin [a]

[a] *Department of Nuclear, Plasma and Radiological Engineering, University of Illinois at Urbana Champaign, 216 Talbot Lab, 104 S. Wright Street, Urbana, IL 61801, USA*

[b] *Argonne National Laboratory, 9700, S. Cass Ave, Darien, IL 60439, USA*

ARTICLE INFO

Keywords:
Multiphase
Peng–Robinson equation of state
Surface tension

ABSTRACT

This paper presents a consistent LBM formulation for the simulation of a two-phase water–steam system. Results of initial model validation in a range of thermodynamic conditions typical for Boiling Water Reactors (BWRs) are also shown. The interface between the two coexisting phases is captured from the dynamics of the model itself, i.e., no interface tracking is needed. The model is based on the Peng–Robinson (P–R) non-ideal equation of state and can quantitatively approximate the phase-coexistence curve for water at different temperatures ranging from 125 to 325 °C. Consequently, coexisting phases with large density ratios (up to ∼1000) may be simulated. Two-phase models in the 200–300 °C temperature range are of significant importance to nuclear engineers since most BWRs operate under similar thermodynamic conditions. Simulation of bubbles and droplets in a gravity-free environment of the corresponding coexisting phase until steady state is reached satisfies Laplace law at different temperatures and thus, yield the surface tension of the fluid. Comparing the LBM surface tension thus calculated using the LBM to the corresponding experimental values for water, the LBM lattice unit (lu) can be scaled to the physical units. Using this approach, spatial scaling of the LBM emerges from the model itself and is not imposed externally.

1. Introduction

Advances in Computational Fluid Dynamics (CFD) over the last two decades have been very impressive. Several fields of engineering – including aeronautical, automotive, mechanical, chemical, etc. – have benefited from this progress. However, the fruits of this development have been more limited for applications that involve boiling and two-phase flows, such as those in nuclear engineering and some other branches of engineering. The reason may be the slow progress in CFD to accurately model challenging problems of interest such as those that involve boiling or multiphase flows. A specific example is the Boiling Water Reactor (BWR) core, in which the coolant enters the core as liquid, undergoes a phase change as it traverses the core and exits as a high quality two-phase mixture. Two-phase flows in BWRs typically manifest a wide variety of geometrical patterns of the co-existing phases depending on the local system conditions. Modeling of such flows currently relies on empirical correlations (for example, in the simulation of bubble nucleation, bubble growth and coalescence, and inter-phase surface topology transitions) that hinder the accurate simulation of two-phase phenomena using Computational Fluid Dynamics (CFD) type approaches. While the level-set method (LSM) and the volume-of-fluid method (VOF) [1–3] have successfully been applied to model certain two-phase systems, there is still a need for alternative approaches to

* Corresponding author.
E-mail addresses: pkjain2@uiuc.edu (P.K. Jain), tentner@anl.gov (A. Tentner), rizwan@uiuc.edu (Rizwan-uddin).

0898-1221/$ – see front matter © 2009 Elsevier Ltd. All rights reserved.
doi:10.1016/j.camwa.2009.02.004

understand the connection between the two-phase macroscopic phenomena and their underlying microscopic dynamics at a much more fundamental level. Ideally, molecular dynamics (MD) simulations may be the key to accurately predict these phenomena. However, MD is not yet ready to be exploited for large scale applications due to extremely high computational cost associated with such simulations. Thus, a methodology which can bridge the gap between molecular dynamics and macroscopic simulations may be more suitable for the present state of computational power. The Lattice Boltzmann Method (LBM) is a good candidate because of its remarkable potential to simulate single- and multiphase fluids at mesoscopic levels with affordable computational expense [4,5]. The uniqueness of the LBM approach is that macroscopic dynamic phenomena evolve through the simulation of the microscopic physics of the system [6–9].

In this paper, we present a methodology to simulate a two-phase system of a single-component fluid (such as liquid water and steam) with large phase density ratios. An inter-particle potential model proposed by Zhang and Chen [10] is used in this study to segregate the two coexisting phases. Moreover, the Peng–Robinson (P–R) non-ideal equation of state is used to model the saturation densities of water and steam. The Exact Difference Method (EDM) proposed by Kupershtokh [11,12] is employed to account for body forces in the LBM algorithm. The surface tension of the water and steam mixture is predicted by simulating a series of bubbles/drops with different radii. Comparing the surface tension of the LBM simulations with those of experimental data, the LBM grid size is estimated in real physical units.

2. Methodology

In the LBM, the evolution of "particles" takes place in the following two sequential steps: (a) streaming, in which the particles propagate from a given node, according to their velocity direction, to the neighboring nodes; and (b) collision, in which particles arriving at a particular node collide and change their velocity directions following some simple scattering rules. During the collision step, the direction-specific density distributions of particles are relaxed towards local equilibrium. An important feature of this approach is that the rules governing the propagation and collisions are designed such that the coarse-grained motion of particles is consistent with the Navier–Stokes equations. Various boundary conditions are easily incorporated. They include not only the standard single-phase flow boundary conditions, but boundary conditions for multiphase systems, such as the pressure drop across interfaces and fluid–solid-interface wetting effects as well [13–22].

2.1. D_2Q_9 Scheme with LBGK approximation

The Lattice Boltzmann equation with streaming and single relaxation time collision operator (often known as BGK approximation [18]) is

$$f_a(\mathbf{x} + \mathbf{e_a}\Delta t, t + \Delta t) = f_a(\mathbf{x}, t) + \frac{[f_a^{\mathrm{eq}}(\mathbf{x}, t) - f_a(\mathbf{x}, t)]}{\tau} \tag{1}$$

where $f_a(\mathbf{x}, t)$ is the streaming part and $\frac{[f_a^{\mathrm{eq}}(\mathbf{x},t)-f_a(\mathbf{x},t)]}{\tau}$ is the collision part. Here, f_a is the density of particles in the "a" direction, and f_a^{eq} is the equilibrium distribution function. Moreover, $\mathbf{x}$ is position vector, $\mathbf{e_a}$ are velocity vectors, t is time, Δt is the time step, and τ is the relaxation time that captures the kinematic viscosity ν of the fluid given by $\nu = \frac{2\tau-1}{6}$. On a simple D_2Q_9 lattice (2D lattice with 8 velocity directions and 1 rest state), the equilibrium distribution function f_a^{eq} is defined as [4,5]

$$f_a^{\mathrm{eq}}(\mathbf{x}, t) = f_a^{\mathrm{eq}}(\rho(\mathbf{x}, t), \mathbf{u}(\mathbf{x}, t)) = w_a\rho(\mathbf{x}, t)\left[1 + 3\frac{\mathbf{e_a}.\mathbf{u}}{c^2} + \frac{9}{2}\frac{(\mathbf{e_a}.\mathbf{u})^2}{c^4} - \frac{3}{2}\frac{\mathbf{u}^2}{c^2}\right] \tag{2}$$

where the weights w_a are 4/9 for the rest particles ($a = 0$), 1/9 for $a = 1, 2, 3, 4$, and 1/36 for $a = 5, 6, 7, 8$, and $\sqrt{2}c$ is the maximum attainable macroscopic speed on the lattice. Macroscopic variables such as the fluid density ρ and velocity $\mathbf{u}$ are obtained in terms of $f_a(\mathbf{x}, t)$:

$$\rho(\mathbf{x}, t) = \sum_{a=0}^{8} f_a(\mathbf{x}, t) \tag{3}$$

$$\mathbf{u}(\mathbf{x}, t) = \frac{1}{\rho(\mathbf{x}, t)}\sum_{a=0}^{8} f_a(\mathbf{x}, t)\mathbf{e_a}. \tag{4}$$

2.2. Particle interaction potential and force

In order to simulate two coexisting phases in equilibrium, an inter-particle potential model proposed by Zhang and Chen [10] is implemented. A non-ideal equation of state $p(\rho, T)$ (such as the Peng–Robinson equation of state for water and

steam) is incorporated in this model by expressing the particle interaction force as the spatial gradient of a scalar function $U(\mathbf{x}, t)$,

$$F_{\text{int}}(\mathbf{x}, t) = -\nabla U(\mathbf{x}, t). \tag{5}$$

$U(\mathbf{x}, t)$ is chosen to satisfy

$$U(\mathbf{x}, t) = p(\rho(\mathbf{x}, t), T(\mathbf{x}, t)) - \rho(\mathbf{x}, t)c_s^2 \tag{6}$$

in order to yield global momentum conservation. Here c_s^2 is the lattice speed of sound and equal to $c^2/3$ for the D_2Q_9 scheme [10]. Now, by introducing interaction potential $\psi(\mathbf{x}, t)$ as

$$\psi^2(\mathbf{x}, t) = |U(\mathbf{x}, t)| \tag{7}$$

the interaction force $F_{int}(\mathbf{x}, t)$ can be written as

$$F_{\text{int}}(\mathbf{x}, t) = 2\psi(\mathbf{x}, t)\nabla\psi(\mathbf{x}, t). \tag{8}$$

In the above equations, the interaction potential (and force) depends upon the spatial and temporal grids via local density and local temperature governed by the non-ideal equation of state.

2.3. Numerical implementation on a D_2Q_9 lattice

For a grid point (i, j) of a D_2Q_9 lattice, Eq. (8) can be numerically evaluated by taking account of the interaction potentials at its nearest – $(i+1, j)$, $(i-1, j)$, $(i, j+1)$, $(i, j-1)$ – and the next-nearest – $(i+1, j+1)$, $(i-1, j-1)$, $(i+1, j-1)$, $(i-1, j+1)$ – neighbor sites. This leads to a six point scheme for the potential gradient in x- and y-directions, and may be written as [22],

$$\begin{aligned}\frac{\partial\psi}{\partial x}(i, j) &= w_{\text{near}}[\psi(i+1, j) - \psi(i-1, j)] \\ &\quad + w_{\text{next-near}}[\psi(i+1, j+1) - \psi(i-1, j+1) + \psi(i+1, j-1) - \psi(i-1, j-1)] \qquad (9)\\ \frac{\partial\psi}{\partial y}(i, j) &= w_{\text{near}}[\psi(i, j+1) - \psi(i, j-1)] \\ &\quad + w_{\text{next-near}}[\psi(i+1, j+1) - \psi(i+1, j-1) + \psi(i-1, j+1) - \psi(i-1, j-1)]. \qquad (10)\end{aligned}$$

To find the weighting coefficients w_{near} and $w_{\text{next-near}}$, the potential gradient may be approximated by using the method of finite difference in the x-direction (assuming $\Delta x = \Delta y = 1$),

$$\begin{aligned}\frac{\partial\psi}{\partial x}(i, j) &= \frac{1}{2}[\psi(i+1, j) - \psi(i-1, j)] \\ &= \frac{1}{4}[(\psi(i+1, j+1) + \psi(i+1, j-1)) - (\psi(i-1, j+1) + \psi(i-1, j-1))]. \qquad (11)\end{aligned}$$

In the above equation, a second order central finite-difference scheme is used in the x-direction to get the potential gradient at (i, j) in terms of potential values at $(i-1, j)$ and $(i+1, j)$. These neighboring node potentials are further approximated by averaging the corresponding potential values of the neighboring nodes in the y-direction. The equation for the potential gradient in the y-direction can also be written in a similar way. From Eqs. (9) and (11), it is clear that the correct determination of weighting coefficients requires,

$$w_{\text{near}} + 2w_{\text{next-near}} = \frac{1}{2} \tag{12}$$

and $w_{\text{near}} > w_{\text{next-near}}$ since nearest neighbors should have more influence when compared to the next-nearest neighbors. For the LBM simulations reported here, w_{near} and $w_{\text{next-near}}$ are chosen to be $w_{\text{near}} = 4w_{\text{next-near}} = \frac{1}{3}$ [22].

There is a need for some flexibility in predicting the same coexistence curve from the LBM simulations using different equations of state. To provide this flexibility, a parameter ξ is inserted into the expression for the interaction force by approximating $\psi(\mathbf{x}, t)$ that appears in Eq. (8), for example, in the x-direction as

$$\psi_{approx}(i, j) = \xi(\psi(i+1, j) + \psi(i-1, j)) + (1 - 2\xi)\psi(i, j). \tag{13}$$

Depending upon the equation of state being modeled, a ξ value may be determined that leads to LBM results that accurately match the theoretical saturated densities for both the phases [11]. For the simulations reported in this paper, the ξ value is chosen as -0.088 in order to yield good agreement with the theoretical coexistence curve constructed using the Peng–Robinson (P–R) equation of state (described later in Section 3). Several numerical experiments of spinodal decomposition phase-segregation are carried out at the same temperature with different ξ values in the simulations and then the appropriate ξ value is chosen for which the resulted saturated densities are in close agreement with the theoretically obtained (using the Maxwell construction on the P–R equation of state) saturated densities of liquid and vapor phases. While performing numerical experiments it is observed that the parameter ξ only needs to be tuned once at any selected temperature in the coexistence region and then may be used for other temperatures as a constant to yield results in good agreement with the theoretical ones.

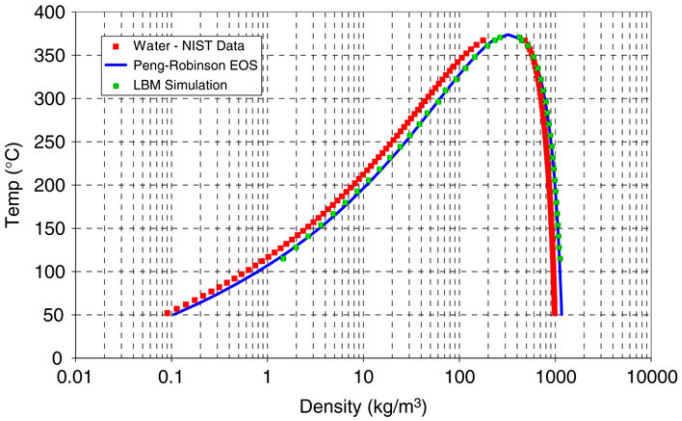

Fig. 1. Comparison of the theoretical coexistence curve (Maxwell construction) and the corresponding LBM simulation for Peng–Robinson (P–R) equation of state. Saturated water and vapor densities from NIST tables [20] are also shown.

3. Simulation of body forces

In the LBM, the incorporation of body forces (particle interaction, gravitational or externally applied forces) usually affects the stability of multiphase simulations. Numerical instability is caused due to large changes in velocity in the interface region during each time step. In order to increase the stability of the LBM simulations, an Exact Difference Method (EDM) is proposed by Kupershtokh [12] which combined with the general approximation of forcing functions results in reduced spurious currents at the interfaces and accurate reproduction of the phase-coexistence curve. In EDM, a term Δf_a representing the change in the distribution function is added to the collision term to account for the change in momentum due to body forces. Thus, at the time step $(t + \Delta t)$

$$f_a(\mathbf{x} + \mathbf{e_a}\Delta t, t + \Delta t) = f_a(\mathbf{x}, t) + \frac{[f_a^{\mathrm{eq}}(\mathbf{x}, t) - f_a(\mathbf{x}, t)]}{\tau} + \Delta f_a \tag{14}$$

where Δf_a equals to the difference in the equilibrium distribution function evaluated at the constant density as the velocity is varied for each time-step Δt, and is given by,

$$\Delta f_a = f_a^{\mathrm{eq}}(\rho, \mathbf{u} + \mathbf{\Delta u}) - f_a^{\mathrm{eq}}(\rho, \mathbf{u}). \tag{15}$$

Here, change in velocity $\mathbf{\Delta u}$ is evaluated by computing the change in momentum $\mathbf{\Delta p}$ at each time-step due to body forces, and is given by

$$\mathbf{\Delta u} = \frac{\mathbf{\Delta p}}{\rho} = \frac{\mathbf{F}(\mathbf{x}, t)\Delta t}{\rho}. \tag{16}$$

4. Peng–Robinson (P–R) equation of state

An equation of state (EOS) describes the relationship between temperature, pressure and density (volume) of a fluid. One such EOS is the Peng–Robinson (P–R) equation of state [19] that is widely used for determining the state of various fluids categorized by different accentric factors. The accentric factor (ω) depends on the molecular structure of the fluid and is determined from its critical properties. Values of ω are tabulated in thermodynamic tables for various fluids. P–R EOS, which is a three-parameter (T_c, p_c and ω, defined below) cubic equation, fairly accurately captures the saturated densities over most of the liquid–vapor equilibrium curve. For water and steam, the accentric factor $\omega = 0.3443$ leads to predicted values of saturated densities that agree very well with experimental data. This comparison is shown in Fig. 1. Although more sophisticated equations of state – fitted to experimental data – can be developed and implemented in the LBM model, the P–R EOS is chosen due to its flexibility in changing the type of fluid by varying the accentric factor ω.

The P–R equation of state is:

$$p = \frac{\rho RT}{1 - b\rho} - \frac{a\alpha(T)\rho^2}{1 + 2b\rho - b^2\rho^2} \tag{17}$$

where $\alpha(T) = [1+(0.37464+1.54226\omega-0.26992\omega^2)(1-\sqrt{T/T_c})]^2$ and $a = 0.45724R^2T_c^2/p_c, b = 0.0778RT_c/p_c$. Here, T_c and p_c represent critical temperature and critical pressure of the fluid under consideration, respectively. For water, T_c is 647.1 K and p_c is 22.064 MPa. In simulations reported here, the constants a, b and R are set to be 2/49, 2/21 and 1, respectively. The

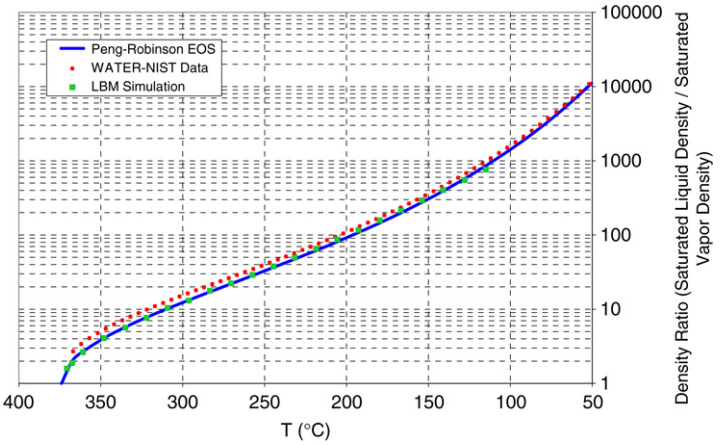

Fig. 2. Comparison of density ratios (saturated water/saturated vapor) obtained from Peng–Robinson EOS, NIST saturated property tables [20], and from corresponding LBM simulations at different temperatures.

Table 1
Comparison of saturated properties of water obtained from NIST tables [20] and LBM simulations at various temperatures.

T/T_c	T (°C)	$\rho_{sat,liquid}$ (kg/m^3)		$\rho_{sat,vapor}$ (kg/m^3)		p_{sat} (MPa)	
		NIST	LBM	NIST	LBM	NIST	LBM
0.60	115.11	945.62	1117.36	1.02	1.46	0.18	0.18
0.62	128.05	937.49	1093.01	1.37	1.98	0.25	0.26
0.64	140.99	924.48	1077.74	2.07	2.66	0.38	0.35
0.66	153.94	915.27	1061.57	2.67	3.60	0.50	0.49
0.68	166.88	900.65	1044.51	3.83	4.85	0.73	0.68
0.70	179.82	885.01	1026.35	5.37	6.49	1.05	0.92
0.72	192.76	874.00	1007.07	6.65	8.61	1.31	1.24
0.74	205.70	856.54	986.53	9.01	11.31	1.79	1.65
0.76	218.65	837.84	964.56	12.03	14.70	2.40	2.16
0.78	231.59	824.63	941.06	14.47	18.91	2.89	2.79
0.80	244.53	803.53	915.81	18.90	24.11	3.77	3.56
0.82	257.47	788.53	888.55	22.47	30.49	4.46	4.47
0.84	270.41	764.36	859.00	28.96	38.28	5.66	5.56
0.86	283.36	746.97	822.79	34.20	46.15	6.60	6.64
0.88	296.30	718.53	793.43	43.82	60.33	8.21	8.36
0.90	309.24	686.48	747.75	56.27	71.51	10.12	9.74
0.92	322.18	662.45	707.96	66.74	92.21	11.56	11.86
0.94	335.12	620.65	657.16	87.37	115.75	14.03	14.01
0.96	348.07	586.88	591.89	106.31	144.42	15.90	16.28
0.98	361.01	516.71	518.09	151.35	195.95	19.09	19.10
0.99	367.48	481.53	445.58	177.15	234.35	20.27	20.55

critical properties of the LBM fluid are then evaluated in terms of these constants. Using the law of corresponding states [19], the reduced properties of lattice fluid can then be converted to real fluid properties.

P–R EOS can be written as a cubic equation in V (replace ρ by $1/V$ in Eq. (17)) and thus, has three real roots for $T < T_c$. The benefit of cubic nature is that it can describe both the gaseous and the liquid phases of a fluid. Plotting p vs. V at constant T and then applying the so-called *Maxwell equal-area construction* [19], yields the phase-coexistence curve. Fig. 1 compares the theoretical coexistence curve with the one obtained using the LBM simulations. It can be seen that the LBM results agree well with the theoretical results. Moreover, in Fig. 1, the saturated water and vapor densities from NIST tables [20] are also plotted for comparison. It is observed that, when compared to the water–steam data at a selected temperature, P–R EOS slightly over-predicts the saturated vapor and water densities. However, the calculated density ratio of saturated liquid and vapor matches very well with the water–steam data at different temperatures as shown in Fig. 2. The saturated properties obtained from NIST data [20] and LBM simulations are compared in Table 1 for different temperatures.

5. Kinematic viscosities of liquid and vapor phases

In the LBM-BGK algorithm, the kinematic viscosity of a fluid ν is explicitly determined by the prescribed single relaxation time τ from the relationship, $\nu = \frac{2\tau-1}{6}$. This functional form gives a unique value for the kinematic viscosity of the fluid

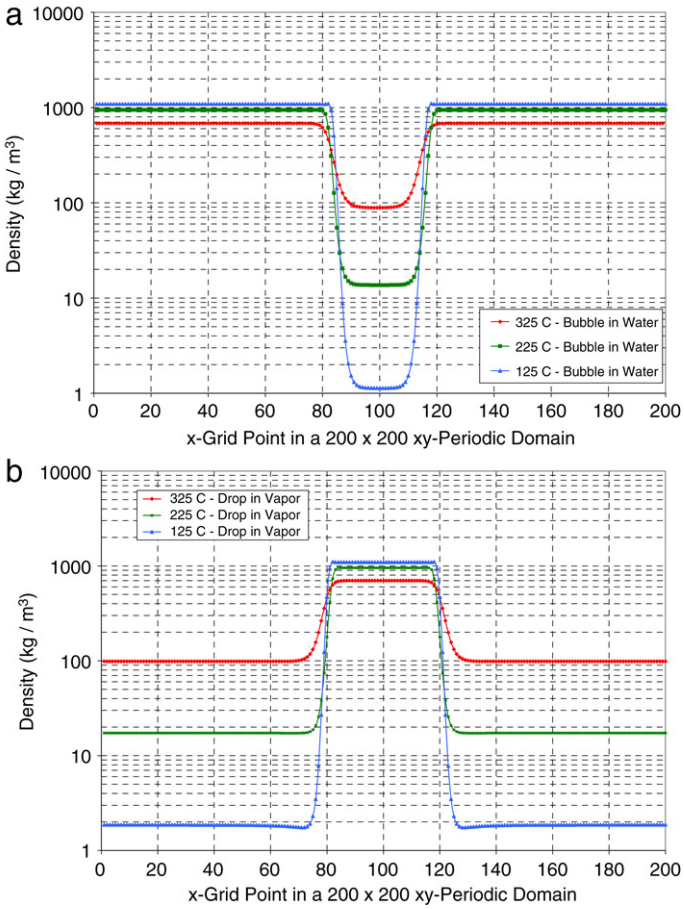

Fig. 3. The LBM simulation of a stationary saturated vapor bubble (saturated liquid drop) in equilibrium with its saturated liquid (saturated vapor) environment at different temperatures. A periodic domain of 200 × 200 grid size is initialized with one phase over a circular shape (of 20 grid-point radius) surrounded by another phase in the remaining space. A total of 40,000 time-steps are simulated to achieve steady state for both cases: (a) *vapor bubble in liquid;* and (b) *liquid drop in vapor*.

irrespective of the multiple phases involved. However, in order to accurately model the flow dynamics of a single-component two-phase fluid, it is essential to have different kinematic viscosities for the two phases at any given temperature. This can be accomplished by expressing the relaxation time τ as a linear function of the local fluid density $\rho(x, y)$ constrained by the saturation densities of both phases [21]. Thus, $\tau(\rho)$ can be written as

$$\tau(\rho) = \left[\frac{\tau(\rho_L) - \tau(\rho_V)}{\rho_L - \rho_V}\right]\rho + \left[\frac{\tau(\rho_V)\rho_L - \tau(\rho_L)\rho_V}{\rho_L - \rho_V}\right] \tag{18}$$

where $\tau(\rho_L)$ and $\tau(\rho_V)$ represent, at the given temperature, the relaxation times corresponding to the saturation density of the liquid and vapor phases, respectively. These phase-specific relaxation times are calculated by knowing the corresponding phase kinematic viscosities.

6. Results and discussion

The LBM simulations are performed for a *xy*-periodic domain of size 200 × 200 lattice units (lu). Initially, a water drop (or vapor bubble) of 20 × 20 lu radius is placed at the centre of the domain surrounded by the corresponding coexisting phase (saturated vapor for liquid *drop at the centre* and saturated liquid for vapor *bubble in the centre*). The simulation is evolved in time till the steady state is reached. After 40,000 time-steps, the difference in simulated observed variables (velocities, densities etc.) for each consecutive 1000 time-steps reaches below 10^{-6} units. This is taken as the criterion for the steady state. Fig. 3 shows the steady-state density variation along a line passing through the centre of the drop (or bubble) for different temperatures. It is observed that the interface between the two phases becomes thicker as temperature increases for both the drop and the bubble.

Using the Laplace law, the surface tension of water–steam system may be estimated. A series of bubbles of various sizes (20 to 50 lu radius) are simulated at different temperatures. After 40,000 time-steps, the steady-state radii and inside/outside

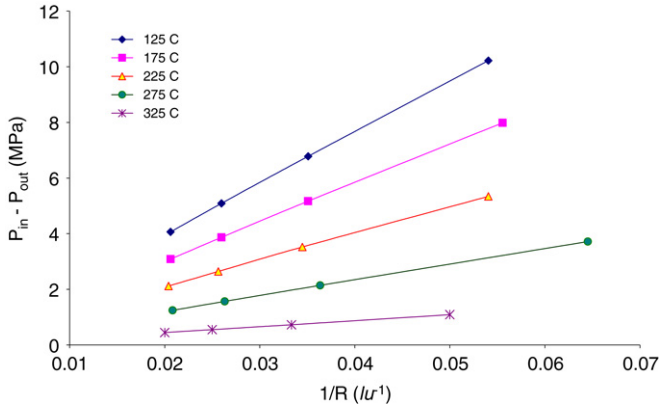

Fig. 4. Plot of pressure difference across bubble vs. inverse radius simulated at different temperatures. Results of the LBM simulations satisfy Laplace law and the slope of curves gives surface tension of the fluid at the respective temperature. Simulation domain is *xy*-periodic, and of 200 × 200 lattice unit size.

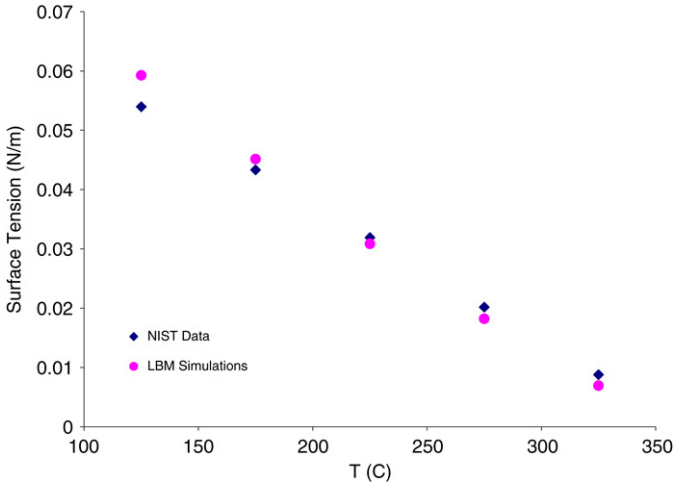

Fig. 5. A comparison of surface tension of water (NIST data) with the surface tension values obtained from the LBM simulations, after lattice scaling.

densities of the bubble are evaluated. Densities are then converted to the corresponding pressures using P–R EOS and the difference between the inside and the outside pressure ΔP of the bubble is computed. According to the Laplace law, for a 2D droplet/bubble, the pressure difference is given by

$$\Delta P = \frac{\sigma}{R}. \tag{19}$$

In Fig. 4, ΔP is plotted against the inverse of the bubble radius $(1/R)$ which yields straight lines of different slopes at different temperatures. As can be seen from Fig. 4, the spatial grid resolution of the LBM fluid is still in the lattice units (lu). Therefore, comparing the LBM surface tension (slope of ΔP vs. $1/R$) with experimental surface tension of water may give an approximate measure of the LBM grid size in physical units. Thus, we can write

$$\sigma_{\text{LBM,lu}}(\text{MPa lu}) = f\sigma_{\text{Water}}\ (\text{Pa m}) \tag{20}$$

where $\sigma_{\text{LBM,lu}}$ is the LBM surface tension in MPa-lu units and σ_{Water} is the water surface tension in *Pa-m* units, for example, as given by NIST. Here, f is a scaling factor with appropriate units to relate both the surface tensions. From Eq. (20), the estimate for 1 lattice unit in LBM is obtained as:

$$1\ \text{lu} = f \times 10^{-6}\ \text{m}. \tag{21}$$

With f close to $1/3000$, the LBM surface tension when converted to physical units well predicts the surface tension values in NIST tables for water for different temperatures ranging from 125 to 325 °C. For water, 1 lattice unit is hence estimated to be close to 0.33 nm. Fig. 5 and Table 2 show comparison of the surface tensions of the LBM fluid and the values tabulated in NIST water property table (after the spatial scaling). Good agreement with macroscopic values suggests that the LBM approach is able to capture the surface tension phenomenon rather well at this scale. However, such a small lattice size is a concern

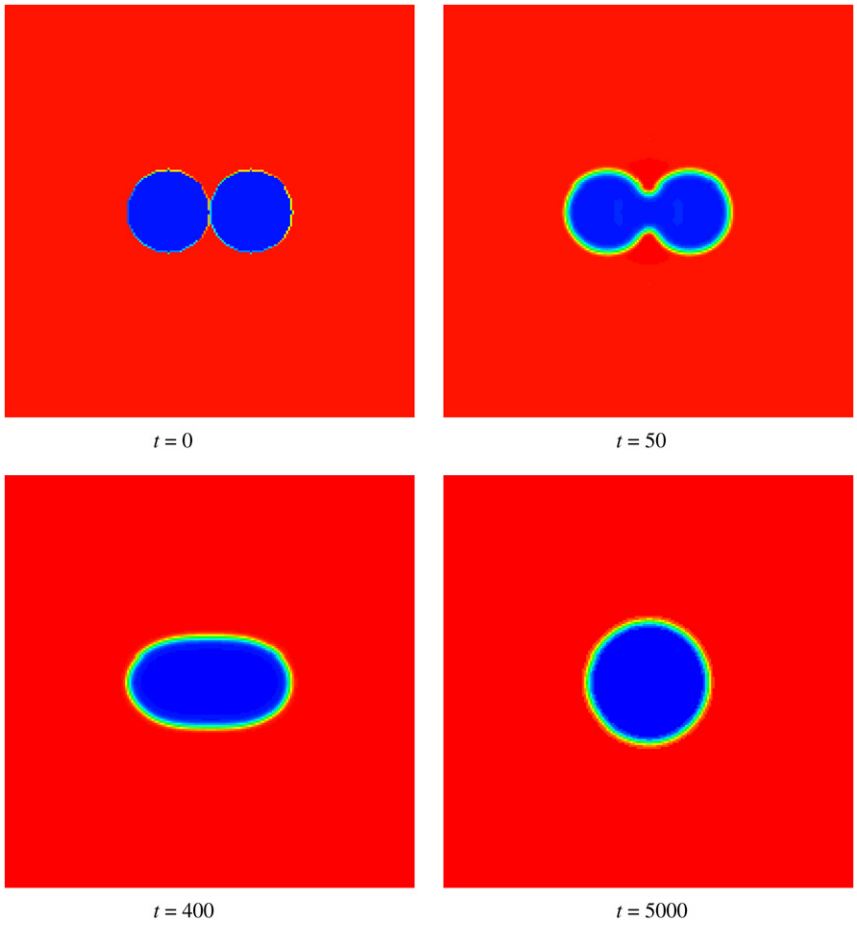

Fig. 6. Snapshots showing coalescence of 2D vapor bubbles at $T = 250\ ^\circ$C. Densities of bubble (shown in blue) and liquid (shown in red) are 23.093 and 896.214 kg/m^3, respectively. Ratio of kinematic viscosity of vapor and liquid is 6.5 [20]. (For interpretation of the references to colour in this figure legend, the reader is referred to the web version of this article.)

Table 2
Comparison of surface tension of water obtained from NIST tables [20] and LBM simulations at various temperatures.

T (°C)	σ (N/m)	
	NIST	LBM
125	0.053955	0.059265
175	0.043302	0.045139
225	0.031903	0.030836
275	0.020163	0.018221
325	0.008774	0.006924

for the computational viability of any realistic simulation and future work will refine the LBM model to allow capturing the correct surface tension while using a coarser lattice.

Next, some qualitative results for the two-phase test simulations performed in a zero-gravity periodic domain of 200×200 lattice dimension are presented. The local densities are allowed to evolve according to the LBM algorithm at a specified temperature until the steady state is reached. Simulations are performed at a temperature of 250 °C at which the coexisting phase density ratio equals ∼40. This temperature and the corresponding density ratio are of prime interest to nuclear engineers since most of the Boiling Water Reactors (BWRs) operate at this mean temperature. In Fig. 6, different stages of a coalescence process of two vapor bubbles (2D) are shown. Initially, at $t = 0$, the bubbles are separated by a very thin liquid layer of 1 lu thickness. As time evolves, the bubbles start coalescing with each other to minimize the net

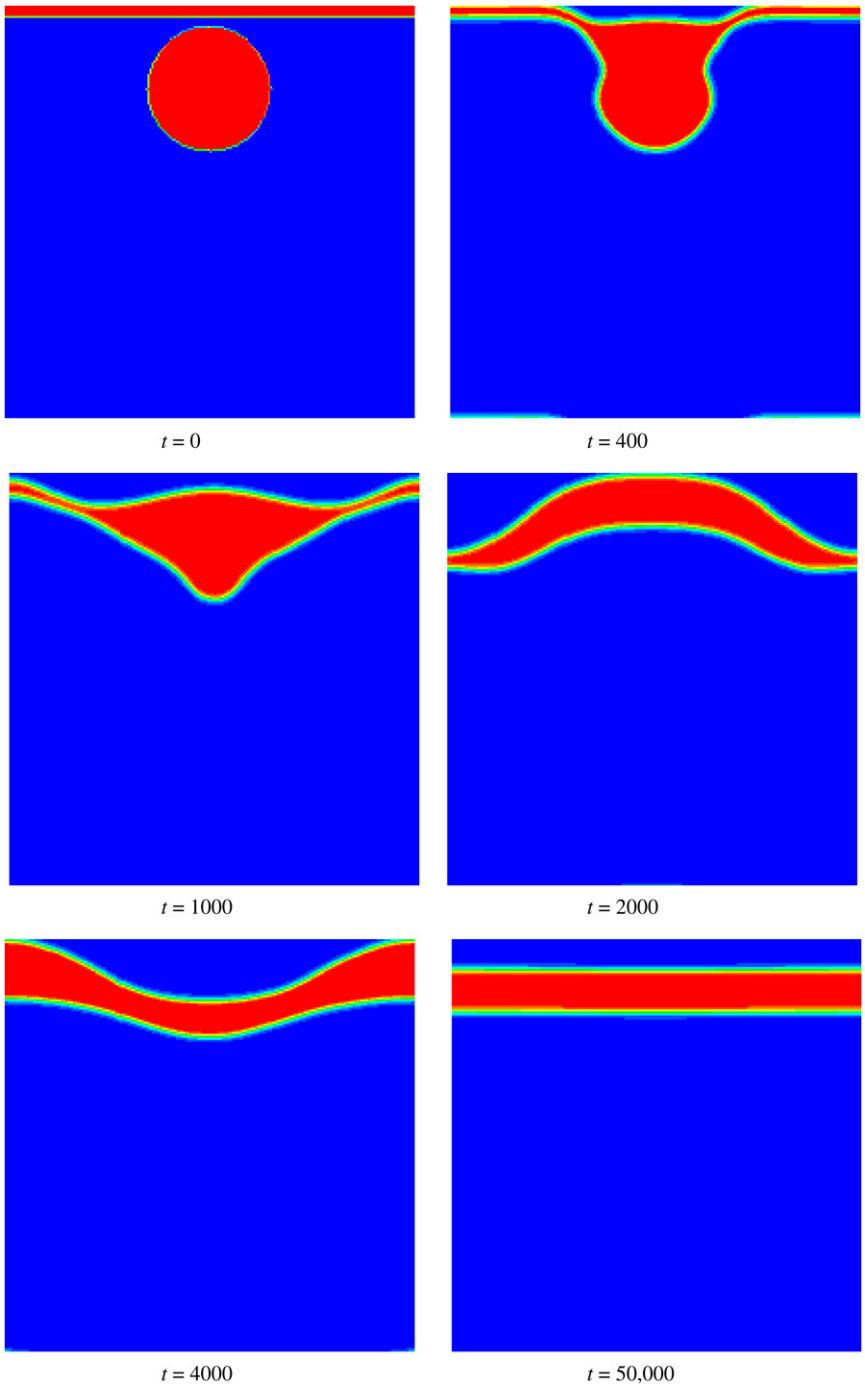

Fig. 7. Snapshots showing coalescence of a thin liquid film with a liquid droplet at different LBM time-steps for $T = 250\,^{\circ}\mathrm{C}$. Densities of vapor (shown in blue) and liquid drop or film (shown in red) are 23.093 and 896.214 kg/m^3, respectively. Ratio of kinematic viscosity of vapor and liquid is 6.5 [20]. (For interpretation of the references to colour in this figure legend, the reader is referred to the web version of this article.)

interfacial energy and finally, leading to a single large bubble of area *approximately* equal to the sum of the areas of initial bubbles.

In Fig. 7, results of a simulation that models the interaction between a liquid film and a liquid droplet are shown. Initially, at $t = 0$, there exists a thin vapor film between the liquid film and the droplet. As time evolves, the drop experiences a cohesive force from the film and attaches to it. Now, the combined liquid chunk oscillates and reorganizes itself to minimize the net interfacial energy by minimizing its surface area. Finally, it leads to a thick liquid film of volume equal to the sum of

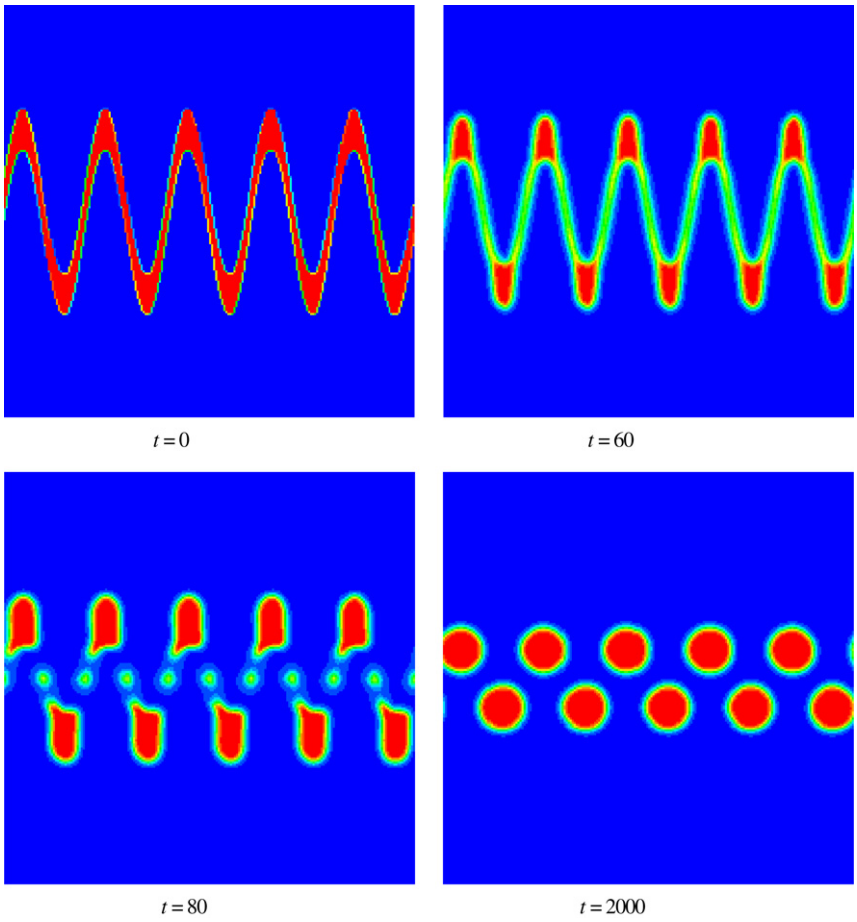

Fig. 8. Snapshots showing break-up of a sinusoidal thin liquid film of large wave amplitude into several circular droplets ($T = 250\,^{\circ}$C). Densities for vapor (shown in blue) and liquid (shown in red) are 23.093 and 896.214 kg/m^3, respectively. Ratio of kinematic viscosity of vapor and liquid is 6.5 [20]. (For interpretation of the references to colour in this figure legend, the reader is referred to the web version of this article.)

the volumes of the liquid film and the droplet. In Figs. 8 and 9, results are shown for a thin liquid film of sinusoidal shape as it evolves after a sudden relaxation in the absence of any external force. By prescribing the sinusoidal shape as an initial condition, the system contains very high interfacial energy and tries to minimize it during relaxation to equilibrium in time. The evolution scenario is simulated for two different cases with equal film thickness and different oscillation amplitudes. In the case of a large amplitude sinusoidal wave, the film breaks up into several circular droplets (Fig. 8), while a relatively small amplitude wave dampens out and evolves into a liquid film of uniform thickness (Fig. 9).

7. Conclusions

It is shown that a non-ideal equation of state, such as the Peng–Robinson EOS, may be coupled with the LBGK scheme with a single density-dependent relaxation time to capture the phase-coexistence curve for water and steam in a wide range of temperatures. Simulating a series of isothermal bubbles and droplets suspended in their coexisting phase predicts the surface tension of the LBM fluid. Comparing this to the experimental data for water provides a way to scale the spatial grid of the LBM in physical units so that the predicted surface tension in physical units accurately matches the measured surface tension data.

Acknowledgements

This research is supported in part by Department of Energy — Innovations in Nuclear Infrastructure and Education (INIE) and Nuclear Engineering Education Research (NEER) grants.

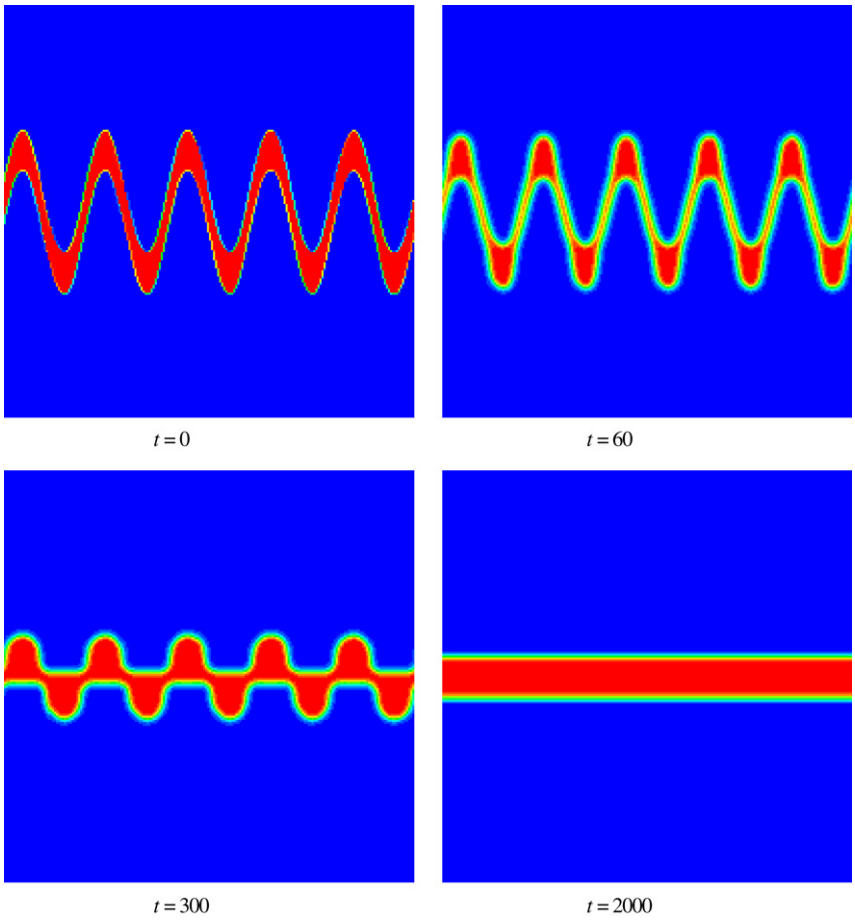

Fig. 9. Snapshots showing relaxation of a sinusoidal thin liquid film of small wave amplitude into a thick liquid film ($T = 250\,^{\circ}\mathrm{C}$). Densities for vapor (shown in blue) and liquid (shown in red) are 23.093 and 896.214 kg/m^3, respectively. Ratio of kinematic viscosity of vapor and liquid is 6.5 [20]. (For interpretation of the references to colour in this figure legend, the reader is referred to the web version of this article.)

References

[1] J.A. Sethian, P. Smereka, Level set methods for fluid interfaces, Annu. Rev. Fluid Mech. 35 (2003) 341–372.
[2] S. Gihun, Efficient implementation of a coupled level-set and volume-fluid-method for three-dimensional incompressible two-phase flows, Numer. Heat Transfer, Part B: Fundamentals 43 (6) (2003) 549–565.
[3] M. Sussman, E.G. Puckett, A coupled level set and volume-of-fluid method for computing 3D and axisymmetric incompressible two-phase flows, J. Comput. Phys. 162 (2) (2000) 301–337.
[4] M.C. Sukop, D.T. Thorne Jr., Lattice Boltzmann Modeling—An Introduction for Geoscientists and Engineers, Springer-Verlag, Berlin, Heidelberg, 2006.
[5] S. Succi, The Lattice Boltzmann Equation—for Fluid Dynamics and Beyond, Oxford Science Publications, UK, 2001.
[6] X. Shan, H. Chen, Lattice Boltzmann model for simulation flows with multiple phases and components, Phys. Rev. E 47 (1993) 1815.
[7] X. Shan, H. Chen, Simulation of nonideal gases and liquid-gas phase transitions by the lattice Boltzmann equation, Phys. Rev. E 49 (1994) 2941.
[8] S. Chen, G.D. Doolen, Lattice Boltzmann method for fluid flows, Annu. Rev. Fluid Mech. 30 (1998) 329.
[9] X. Shan, G.D. Doolen, Multicomponent Lattice-Boltzmann model with interparticle interaction, J. Stat. Phys. 81 (1995) 379.
[10] R. Zhang, H. Chen, Lattice Boltzmann method for simulation of liquid-vapor thermal flows, Phys. Rev. E 67 (2003) 066711.
[11] D. Medvedev, A. Kupershtokh, D. Karpov, On equations of state in a lattice Boltzmann method, in: Talk at: Fourth International Conference for Mesoscopic Methods in Engineering and Science, ICMMES, Munich, Germany, July 16–20, 2007.
[12] A.L. Kupershtokh, New method of incorporating a body force term into the lattice Boltzmann equation, in: Proceedings of the 5th International EHD Workshop, Poitiers-France, Aug 30–31, 2004, pp. 241–246.
[13] A. Tentner, H. Chen, R. Zhang, Simulation of two-phase flow and heat transfer phenomena in a boiling water reactor using the lattice Boltzmann method, Phys. A 362 (2006) 98–104.
[14] P.K. Jain, Rizwan-uddin, A 3D, parallel LBM to simulate gravity driven bubbly and slug flows, Trans. ANS 97, in: Annual Winter Meeting and Technology Expo, Washington DC, USA, Nov. 11–15, 2007.
[15] P.K. Jain, Rizwan-uddin, LBM for nuclear engineers, in: Talk at: Fourth International Conference for Mesoscopic Methods in Engineering and Science, ICMMES, Munich, Germany, July 16–20, 2007.
[16] P.K. Jain, Rizwan-uddin, Lattice Boltzmann method (LBM) for nuclear engineering applications, Trans. ANS 96, in: Annual Summer Meeting and Technology Expo, Boston MA, USA, 2007, pp. 595–597.
[17] P.K. Jain, S. Singh, Y. Yan, Rizwan-uddin, Advanced computing to bridge micro and macro: LBM, advanced CFD and coupled CFD-system codes, in: Poster at: Computational Engineering and Science Conference, CESC-2007, Washington DC, USA, April 10–12, 2007.
[18] P.L. Bhatnagar, E.P. Gross, M.K. Krook, A model for collision process in gases. I. Small amplitude process in charged and neutral one-component system, Phys. Rev. 94 (3) (1954) 511–525.
[19] D. McQuarrie, J.D. Simon, Molecular Thermodynamics, University Science, Sausalito, CA, 1999.

[20] A.H. Harvey, A.P. Peskin, S.A. Klien, NIST/ASME Steam Properties, version 2.21, US Department of Commerce, Technology Administration, National Institute of Standards and Technology, 2004.
[21] A.D. Angelopoulos, V.N. Paunov, V.N. Burganos, A.C. Payatakes, Lattice Boltzmann simulation of nonideal vapor-liquid flow in porous media, Phys. Rev. E 57 (3) (1998) 3237–3245.
[22] P. Yuan, L. Schaefer, Equations of state in a lattice Boltzmann model, Phys. Fluids 18 (2006) 042101.